RECENT APPLICATIONS OF ADVANCED COMPUTATIONAL METHODS IN THE AERODYNAMIC DESIGN OF TRANSPORT AIRCRAFT CONFIGURATIONS

F. T. Lynch*
Douglas Aircraft Company, McDonnell Douglas Corporation
Long Beach, California

Abstract

A new, improved version of the Cebeci-Kaups-Ramsey (CKR) three-dimensional finite-difference boundary-layer program for arbitrary wings has been coupled with the Jameson-Caughey full potential transonic flow method in order to predict the combined viscous/inviscid flow characteristics of three-dimensional swept wings at transonic conditions. Some preliminary computed results are presented for two advanced transport wing configurations. The calculated three-dimensional results are compared with experimental results and with calculations obtained by using the two-dimensional-strip-theory approximation. Limitations of the current method and areas requiring further study are discussed.

Symbols

A	Van Driest damping length
AR	wing aspect ratio — based on trapezoidal portion of wing
c	local chord length
$\bar{c}$	mean aerodynamic chord
c_d	section drag coefficient
C_D	drag coefficient, $D/q_\infty S$
c_f	skin-friction coefficient
c_{f_t}	total skin-friction coefficient
c_ℓ	section lift coefficient
C_L	lift coefficient, $L/q_\infty S$
$C_{L_{expd}}$	exposed wing lift coefficient, $L_{expd}/q_\infty S$
$\mathcal{L}$	centerline
C_p	pressure coefficient, $(p - p_\infty)/q_\infty$
D	drag
H	total enthalpy
K_{12}, K_{21}	geometric parameters
L	lift or modified mixing length
M	Mach number
P	static pressure
Pr	Prandtl number
q_∞	freestream dynamic pressure, $1/2\ \rho_\infty U_\infty^2$
Re	Reynolds number
S	reference area
t	airfoil or wing thickness
u	component of velocity vector in x-coordinate direction
U_∞	freestream velocity
v	component of velocity vector normal to surface
w	component of velocity vector in z-coordinate direction
$-\rho\overline{u'v'}$, $-\rho\overline{w'v'}$, $-\rho\overline{v'H'}$	Reynolds stresses
x	independent variable in chordwise direction
y	independent variable normal to the surface
z	independent variable in spanwise direction
α	angle of attack
β	flow deflection angle
δ	boundary-layer thickness
δ^*	displacement thickness
Δ	displacement surface height
ΔC_{D_C}	incremental drag coefficient due to compressibility
$\Delta C_{P_{SHOCK}}$	increase of pressure coefficient through shock wave
ϵ_m	eddy viscosity
η	wing semispan fraction
θ	angle in tangent plane between x- and z-coordinate lines
θ	momentum thickness
μ	dynamic viscosity
ν	kinematic viscosity
ρ	density
τ	shear stress
Λ	wing sweep

Subscripts

e	boundary-layer outer edge
EST	estimated
L	local
t	total
w	wall
∞	freestream conditions

bars denote Cartesian coordinate system

1. Introduction

Aerodynamic designers of transport aircraft have been dreaming for decades of being able to use, for high-speed design problems, some of the advanced computational tools that they now have available to them such as the three-dimensional transonic flow methods and three-dimensional finite-difference boundary-layer methods. It is anticipated by the designer and his management that the appropriate use of these new advanced computational methods on the wing design of the next subsonic transport aircraft configuration will typically result in an improved aerodynamic technology level, an improved aerodynamic efficiency for a given level of aerodynamic technology, and reduced design costs through a reduction in the amount of wind tunnel testing required and the resulting shortened time period required to define the final lines. Of prime importance in the design of a wing for efficient cruise operation is the ability to achieve separation-free flow at cruising conditions and the ability to predict the onset of trailing-edge separation for the determination of the buffet boundary. A review of the aerodynamic performance characteristics at cruising conditions of commercial subsonic jet transports flying today, all of which were designed without the benefit of these advanced computational methods, leads one to believe that the aerodynamic cruise efficiency of all but a couple of today's transports could have been improved measurably for the technology levels existing when they were designed if these advanced computational methods had been available at the time. Furthermore, the exceptions, in terms of aerodynamic efficiency, are probably the best examples to

*Chief Aerodynamics Engineer, Research and Development Programs

illustrate how the proper application of these new advanced computational methods could have resulted in large cost savings for a given level of aerodynamic efficiency.

Several investigators[1-3] have recently reported promising results using three-dimensional transonic flow computational methods, both full-potential and small-disturbance solutions, in conjunction with simple two-dimensional boundary-layer strip-theory approximations to predict the effects of configuration modifications at transonic conditions. For example, Henne and Hicks[1] showed quite good agreement between calculated and measured pressure distributions and drag increments for a modification to a three-dimensional wing using the Jameson-Caughey full-potential method[4]. However, for as many examples as are presented showing good agreement between experiment and essentially inviscid computational methods, one can be sure that there are at least as many other examples where the agreement is poor due to the presence of strong viscous effects. To attack this problem, numerous organizations have been pursuing the coupling of various three-dimensional boundary-layer methods with three-dimensional transonic flow analysis methods[5-8]. The effort at Douglas on this problem has focused primarily on the use of a new, improved version of the Cebeci-Kaups-Ramsey (CKR) three-dimensional finite-difference boundary-layer program in conjunction with a Douglas version of the Jameson-Caughey full-potential program. The new, improved CKR boundary-layer method is a very accurate, versatile and efficient method for the calculation of three-dimensional boundary layers on arbitrary wings. The choice of the Jameson-Caughey full-potential method over a small disturbance method was clear based on the work of Henne and Hicks[1] who showed that the application of small-disturbance-equation solutions was unreliable for thick transport-type wings. No such restrictions are necessary for the Jameson-Caughey method. A complete description of the CKR boundary-layer method and the Douglas version of the Jameson-Caughey full-potential method is not intended in this paper since much of this information has already appeared in the literature[1,4,5]. However, the important aspects of the new, improved CKR boundary-layer method, and aspects of the Jameson-Caughey code particularly relevant to this study, are discussed in Section 2.

The primary purpose of this paper is to present some preliminary results that illustrate the type of guidance the aerodynamic designer can obtain from this combined three-dimensional transonic and viscous computational tool. This is shown in Section 3 by comparing some calculated results with experimental measurements for two wing configurations designed for an advanced transport model. In addition, results of the three-dimensional boundary-layer calculations are compared with results of boundary-layer calculations obtained by using the two-dimensional-strip-theory approximation. Finally, limitations of the current coupled three-dimensional method and other problem areas requiring further work in order to develop this computational method into an even more useful design tool are discussed in Section 4.

2. Computational Methods

2.1 CKR Three-Dimensional Boundary-Layer Calculation Method

A calculation method for three-dimensional boundary layers on arbitrary wings is based on a number of component parts. These include the coordinate system in which the solution is to be found, the means of representing the wing in this coordinate system, the governing boundary-layer equations, the means of specifying the initial and boundary conditions, the model chosen to represent the turbulent stresses present, and the numerical procedure used to generate the solutions. Numerous investigators[5-8] using various combinations of approaches have tackled this problem with varying degrees of success. At Douglas, the work of Cebeci, Kaups and Ramsey (CKR) led to the development of a procedure for arbitrary wings[5] which is unique in many aspects. This procedure proved to be an effective tool when the isobars on the wing surface were approximately parallel to the leading and trailing edges. However, it was demonstrated that in regions of the flow field where there is a significant layer of crossflow opposing the marching direction, oscillations can occur in the generated solution. This is caused by the stability condition on the difference equations not permitting the correct domain of dependence of the differential equation to be utilized at the particular point being computed. This difficulty has been overcome in the current version of the CKR boundary-layer method through the use of a newly developed numerical procedure referred to as the Cebeci-Stewartson (1977) procedure. With this improvement, the latest CKR boundary-layer method is an accurate, efficient, and reliable method for calculating three-dimensional boundary layers on arbitrary wings. In what follows in this section, a brief description of the important features of the CKR boundary-layer method is given.

Coordinate System. The CKR boundary-layer method uses a nonorthogonal coordinate system which is fit to the particular wing being investigated. The CKR coordinate system consists of parallels to the wing root, and points at equal percent chord across the span. A typical grid is illustrated in Figure 1. This coordinate system allows the airfoil section input to be simply read into the computer program. The choice of this coordinate system for boundary-layer calculations was dictated by the fact that aerodynamic data is usually given in terms of percent of chord and percent of semispan location, and by the almost uniform coverage of the wing that is achieved with the chosen coordinate net. It is the coordinate system in which the engineer naturally thinks of a wing. The use of this coordinate system does add additional terms to the boundary-layer equations, but does not make them unduly complicated. And, of course, the user of the program never sees its internal sections or the development that went into it, but only recognizes the ease with which the geometry is specified.

Governing Equations. The governing boundary-layer equations for three-dimensional compressible laminar and turbulent flows in a nonorthogonal

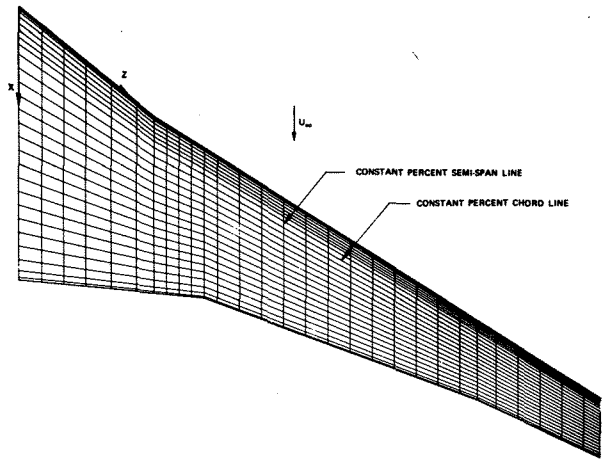

Figure 1. Nonorthogonal Coordinate System Used for Boundary-Layer Calculations on Upper Surface of Advanced Transport Wing.

coordinate system are given by

Continuity equation

$$\frac{\partial}{\partial x}(\rho u h_2 \sin\theta) + \frac{\partial}{\partial z}(\rho w h_1 \sin\theta) + \frac{\partial}{\partial y}(\overline{\rho v} h_1 h_2 \sin\theta) = 0 \qquad (1)$$

x-Momentum equation

$$\rho \frac{u}{h_1}\frac{\partial u}{\partial x} + \rho \frac{w}{h_2}\frac{\partial u}{\partial z} + \overline{\rho v}\frac{\partial u}{\partial y} - \rho \cot\theta\, K_1 u^2 + \rho \csc\theta\, K_2 w^2 + \rho K_{12} uw = -\frac{\csc^2\theta}{h_1}\frac{\partial p}{\partial x} + \frac{\cot\theta \csc\theta}{h_2}\frac{\partial p}{\partial z} + \frac{\partial}{\partial y}\left(\mu \frac{\partial u}{\partial y} - \rho\overline{u'v'}\right) \qquad (2)$$

z-Momentum equation

$$\rho \frac{u}{h_1}\frac{\partial w}{\partial x} + \rho \frac{w}{h_2}\frac{\partial w}{\partial z} + \overline{\rho v}\frac{\partial w}{\partial y} - \rho \cot\theta\, K_2 w^2 + \rho \csc\theta\, K_1 u^2 + \rho K_{21} uw = \frac{\cot\theta \csc\theta}{h_1}\frac{\partial p}{\partial x} - \frac{\csc^2\theta}{h_2}\frac{\partial p}{\partial z} + \frac{\partial}{\partial y}\left(\mu \frac{\partial w}{\partial y} - \rho\overline{w'v'}\right) \qquad (3)$$

Energy equation

$$\rho \frac{u}{h_1}\frac{\partial H}{\partial x} + \rho \frac{w}{h_2}\frac{\partial H}{\partial z} + \overline{\rho v}\frac{\partial H}{\partial y} = \frac{\partial}{\partial y}\left[\frac{\mu}{Pr}\frac{\partial H}{\partial y} + \mu\left(1 - \frac{1}{Pr}\right)\frac{\partial}{\partial y}\left(\frac{u_t^2}{2}\right) - \rho\overline{v'H'}\right] \qquad (4)$$

Here h_1 and h_2 are the metric coefficients and they are, in general, functions of x and z; that is,

$$h_1 = h_1(x,z); \qquad h_2 = h_2(x,z) \qquad (5)$$

Also, θ represents the angle between the coordinates x and z. The parameters K_1 and K_2 are known as the geodesic curvatures of the curves z = const and x = const, respectively. They are given by

$$K_1 = \frac{1}{h_1 h_2 \sin\theta}\left[\frac{\partial}{\partial x}(h_2 \cos\theta) - \frac{\partial h_1}{\partial z}\right], \qquad K_2 = \frac{1}{h_1 h_2 \sin\theta}\left[\frac{\partial}{\partial z}(h_1 \cos\theta) - \frac{\partial h_2}{\partial x}\right] \qquad (6)$$

The parameters K_{12} and K_{21} are defined by

$$K_{12} = \frac{1}{\sin\theta}\left[-\left(K_1 + \frac{1}{h_1}\frac{\partial\theta}{\partial x}\right) + \cos\theta\left(K_2 + \frac{1}{h_2}\frac{\partial\theta}{\partial z}\right)\right] \qquad (7a)$$

$$K_{21} = \frac{1}{\sin\theta}\left[-\left(K_2 + \frac{1}{h_2}\frac{\partial\theta}{\partial z}\right) + \cos\theta\left(K_1 + \frac{1}{h_1}\frac{\partial\theta}{\partial x}\right)\right] \qquad (7b)$$

These equations can be solved when they are expressed in physical coordinates, as above, or in transformed boundary-layer coordinates. In three-dimensional flows, where computer storage and time become quite important, transformed coordinates become necessary, as well as convenient, because they allow the numerical scheme to proceed more efficiently. In addition, they remove the singularity the equations have in physical coordinates at $x = 0$ and $z = 0$. Hence, the equations actually solved in the CKR method are solved in transformed coordinates as described in reference 5.

Initial and Boundary Conditions. In order to generate a solution to equations (1) to (4), initial and boundary conditions must be imposed which specify the exact flow situation being calculated. The boundary conditions are imposed on the wing surface, and in the inviscid flow away from the wing. The conditions imposed on the wing surface are

$$y = 0, \quad u = w = 0, \quad v = v_w, \quad \left(\frac{\partial H}{\partial y}\right)_w = 0 \qquad (8a)$$

where v_w is the specified wall blowing or suction velocity for the calculation of laminar flow control wings. In the inviscid flow, at the edge of the boundary layer,

$$y = \delta, \quad u = u_e(x,z), \quad w = w_e(x,z), \quad H = H_e(x,z) \qquad (8b)$$

where the subscript e denotes quantities at the boundary-layer edge. These values, along with the pressure gradients in equations (2) and (3), are obtained directly from the Jameson-Caughey inviscid calculations for transonic flows and from the Hess panel method for subsonic flows.

The solution of the system given by equations (1) to (4), subject to (8), requires that initial conditions be specified on two planes intersecting the wing along coordinate lines. For a wing, these two planes lie along the leading edge and the root chord. Along the leading edge, stagnation-line equations are used to generate the starting velocity profiles. On the root chord, an approximation must be made because equations (1) to (4) are not valid in this juncture region. In the CKR program, tapered wing equations with no spanwise gradients

are solved, and used as the initial profiles. This procedure works well and does not seem to introduce any spurious effects due to the approximate starting solution.

Turbulence Model. For turbulent flows, it is necessary to make closure assumptions for the Reynolds stresses, $-\rho\overline{u'v'}$, $-\rho\overline{w'v'}$ and $-\rho\overline{v'H'}$. In the current CKR method, as in the previous version, this requirement is satisfied by using the eddy-diffusivity concept and relating the Reynolds stresses to the mean velocity and total enthalpy profiles by

$$-\rho\overline{u'v'} = \rho\varepsilon_m \frac{\partial u}{\partial y} \quad , \quad -\rho\overline{w'v'} = \rho\varepsilon_m \frac{\partial w}{\partial y} \tag{9a}$$

$$-\rho\overline{v'H'} = \rho\varepsilon_H \frac{\partial H}{\partial y} \tag{9b}$$

The CKR method uses the eddy-viscosity formulation of Cebeci[9], and defines ε_m by two separate formulas. In the so-called inner region of the boundary layer, (ε_m) is defined by the following formula

$$(\varepsilon_m)_i = L^2\left[\left(\frac{\partial u}{\partial y}\right)^2 + \left(\frac{\partial w}{\partial y}\right)^2 + 2\cos\theta\left(\frac{\partial u}{\partial y}\right)\left(\frac{\partial w}{\partial y}\right)\right]^{1/2} \tag{10}$$

where

$$L = 0.4y[1 - \exp(-y/A)] \tag{11a}$$

Allowing for flows with pressure gradient and mass transfer

$$A = 26\frac{\nu}{N}\left(\frac{\tau_w}{\rho_w}\right)^{-1/2}\left(\frac{\rho}{\rho_w}\right)^{1/2} \tag{11b}$$

Here

$$\tau_w = u_w\left[\left(\frac{\partial u}{\partial y}\right)_w^2 + \left(\frac{\partial w}{\partial y}\right)_w^2 + 2\cos\theta\left(\frac{\partial u}{\partial y}\right)_w\left(\frac{\partial w}{\partial y}\right)_w\right]^{1/2} \tag{11c}$$

$$N = \left\{\frac{\mu}{\mu_e}\left(\frac{\rho_e}{\rho_w}\right)^2 \frac{p^+}{v_w^+}\left[1 - \exp\left(11.8\frac{\mu_w}{\mu}v_w^+\right)\right] + \exp\left(11.8\frac{\mu_w}{\mu}v_w^+\right)\right\}^{1/2} \tag{11d}$$

$$v_w^+ = \frac{v_w}{u_\tau} \quad , \quad u = \left(\frac{\tau_w}{\rho_w}\right)^{1/2} \quad , \quad p^+ = \frac{\nu_e u_e}{u_\tau^3}\frac{du_e}{dx} \tag{11e}$$

An intermittency factor is then used to account for the transitional region.

In the outer region ε_m is defined by the following formula

$$(\varepsilon_m)_o = 0.0168\left|\int_0^\infty (u_{te} - u_t)dy\right| \tag{12}$$

where

$$u_{te} = (u_e^2 + w_e^2 + 2u_e w_e\cos\theta)^{1/2} \tag{13a}$$

$$u_t = (u^2 + w^2 + 2uw\cos\theta)^{1/2} \tag{13b}$$

The inner and outer regions are established by the continuity of the eddy-viscosity formula. As in the previous version of the CKR method, the turbulent Prandtl number is assumed to be constant and is set equal to 0.9.

Numerical Method. In the CKR boundary-layer method, the Box method is used to solve the boundary-layer equations in transformed coordinates. This is a two-point finite-difference method developed by Keller and Cebeci. This method has been applied to two-dimensional flows as well as three-dimensional flows, and has been found to be efficient and accurate. Descriptions of this method have been presented in a series of papers and reports[5,9,10] and a detailed presentation is contained in a recent book by Cebeci and Bradshaw[11].

The solution procedure used in the last published version of the CKR three-dimensional boundary-layer method[5] employed a marching technique that monitored the edge value of w_e and altered the integration processes based upon the sign of the velocity. As mentioned previously, this procedure was effective for configurations that had isobars nearly parallel to the leading and trailing edges, but encountered difficulties for configurations where the existence of significant spanwise pressure gradients led to significant layers of cross flow opposing the marching direction. The current version of the CKR three-dimensional boundary-layer method uses a new procedure developed by Cebeci and Stewartson in 1977. In this new procedure, which follows the characteristics of the locally plane flow, the direction of w at each grid point across the boundary layer is checked and the difference equations are written accordingly. With this procedure, there is no need to specify any initial conditions along the tip as was required in the previous method[5].

The new method changes the marching procedure previously used so that now an entire spanwise sweep is completed prior to making a further chordwise step. At each point to be calculated, the backward characteristic is computed from the local values of the velocity. It is just these characteristics that determine the domain of dependence. Only information within this domain is used to form the convective derivatives present in the three-dimensional boundary-layer equations. Since the characteristic must be determined as part of the solution, a Newton iteration process is used in the calculation procedure to correctly determine the exact shape of the domain of dependence. Use of this new exact scheme has eliminated the need for the logic included in the previous CKR wing boundary-layer code and results in reduced computer storage requirements. There is no need to change integration direction when reverse crossflows are encountered. The new solution procedure provides accurate and very satisfactory results without any numerical problems as long as the flow is not separated; that is, $u > 0$. Further details of the new numerical solution procedure will be published in a forthcoming paper by Cebeci and Stewartson.

Calculation of Displacement Surface. In order to account for the viscous-inviscid flow interaction, a boundary-layer displacement surface is determined from the output of the boundary-layer

code. The displacement surface height above the surface is given in vector form[12]

$$\operatorname{div}\left[\rho_e \vec{q}_e \Delta - \int_0^{\delta} (\rho_e \vec{q}_e - \rho \vec{q}) dy\right] = h_1 h_2 \sin\theta \, (\rho_w v_w) \tag{14}$$

Here $\vec{q}$ is the vector parallel to the surface and Δ is the displacement surface height. For a non-orthogonal coordinate system, equation (14) becomes

$$\frac{\partial}{\partial x}\left[\rho_e u_e h_2 \sin\theta \, (\Delta - \delta_x^*)\right] + \frac{\partial}{\partial z}\left[\rho_e w_e h_1 \sin\theta (\Delta - \delta_z^*)\right] = h_1 h_2 \sin\theta \, (\rho_w v_w) \tag{15}$$

Here δ_x^* and δ_z^* are the usual definitions of the displacement thicknesses. Equation (15) is a first-order partial-differential equation whose characteristics are the inviscid streamlines. Hence, the solution is obtained by considering the following equivalent system of ordinary differential equations:

$$\frac{dz}{dx} = \frac{w_e h_1}{u_e h_2}$$

$$\frac{d\Delta}{dx} = \frac{1}{\rho_e u_e h_2 \sin\theta}\left\{-\Delta\left[\frac{\partial}{\partial x}(\rho_e u_e h_2 \sin\theta) + \frac{\partial}{\partial z}(\rho_e w_e h_1 \sin\theta)\right] + \frac{\partial}{\partial x}(\rho_e u_e h_2 \sin\theta \delta_x^*) + \frac{\partial}{\partial z}(\rho_e u_e h_1 \sin\theta \delta_z^*)\right\} + \left(\frac{\rho_w v_w}{\rho_e u_e}\right) h_1 \tag{16}$$

Since both the initial data lines are streamlines and consequently characteristics, the solution cannot be continued into the rest of the field with simple marching procedure and equation (16). However, with the solutions on the initial lines known, equation (15) yields the corresponding rates of change of Δ which can be used to construct solutions in the neighborhood of the initial line and then the solutions can be continued in a regular manner using (16).

The calculated displacement surface height is added along the wing surface normal at the nodal points to create a new wing surface. Since the surface normal has, in general, three-dimensional components, the new surface is given by a collection of points from which the wing section coordinates are created by suitable interpolation. The procedure is straightforward provided that the displacement thickness calculation has been completed for every nodal point on the surface. If desired, it is possible to iteratively calculate the boundary-layer solution and the inviscid-flow solution with a displacement surface added at each step. This iterative capability has not been used for the results presented in this paper.

Computation Time. A typical computation time (CPU) for the current CKR three-dimensional compressible boundary-layer method on an IBM 370/165 computer for one surface of a wing with 28 spanwise stations, 30 chordwise stations, and an average of 40 points across the boundary layer, is about 90 seconds.

2.2 Douglas Version of Jameson-Caughey Transonic Full-Potential Method

Although there are numerous efforts underway throughout the world aimed at developing new and improved methods of calculating transonic flow characteristics for general three-dimensional configurations, the current choice of operational methods that can be used to predict the flow characteristics about three-dimensional wings at transonic conditions is between the Jameson-Caughey full-potential method[4] or one of the small-disturbance methods[13,14]. At Douglas, where the emphasis is on transport-type configurations, the choice for prime attention and for coupling with the new, improved version of the CKR three-dimensional boundary-layer program has been the Jameson-Caughey full-potential method. This selection was based on the work of Henne and Hicks' who showed quite clearly that small-disturbance-equation solutions were unreliable for thick transport-type wings. No such restrictions are necessary for the Jameson-Caughey method.

The particular Jameson-Caughey code used for this study is the FLO-22 nonconservative version. This version was selected rather than one of the later ones (FLO-25 or -27) due to the production status of the FLO-22 code and because the general character of pressure distributions predicted by this code, including shock development, strength and location, happen to agree very well with experimental results in many instances. Also, there is a general consensus that the later conservative-form versions will most likely require a modeling of the shock wave- boundary-layer interaction in order for predicted shock locations to match experiment. The following is a brief description of some aspects of the Jameson-Caughey FLO-22 code particularly relevant to this study.

Basic Formulation. The FLO-22 transonic flow method of Jameson and Caughey for three-dimensional wings alone (no fuselage effects) assumes inviscid, adiabatic, and irrotational flow. These assumptions are equivalent to assuming isentropic flow. When entropy changes through shock waves are neglected, the motion of a compressible fluid is well approximated by the well-known full-potential equation. In the J-C method, a finite-difference simulation of the full-potential equation is solved in a mapped coordinate system by using line over-relaxation procedures. The finite-difference simulation employs a nonconservative, rotated difference scheme. The finite-difference solution does not represent shock waves as discontinuities, but instead the shock pressure jump is smeared over several computational mesh widths. Depending on the chordwise and spanwise location, the shock pressure jump can be spread over as much as 10 to 15 percent of the local wing chord. The significance of this smearing of the shock pressure jump is discussed later in the paper.

Mapping Procedure. A mapping procedure is used to accurately impose boundary conditions. The procedure consists of applying a simple conformal transformation in each of one family of coordinate surfaces which almost maps the boundary surfaces to coordinate planes. A shearing transformation is then used to complete the mapping of the boundaries to coordinate surfaces. The final transformation results in a nonorthogonal coordinate system. This mapping procedure results in a concentration of mesh points near the leading edge, and,

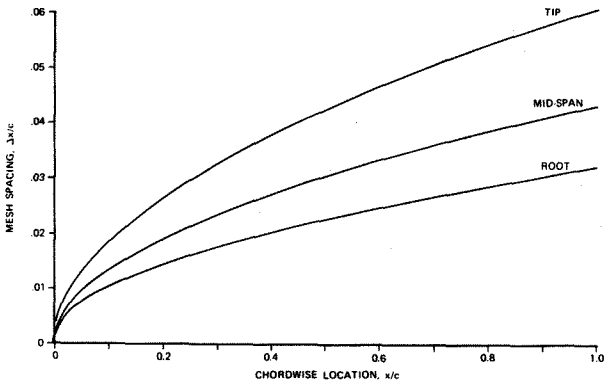

Figure 2. Typical Mesh Spacing for Tapered Wing With J-C FLO-22 Program.

for tapered wings, near the root. The spacing becomes more coarse further aft or further outboard, as illustrated in Figure 2 for a representative tapered wing planform. This coarse spacing, in conjunction with the smearing of the shock pressure jump over several mesh widths, results in the shock pressure jump being smeared over a relatively large chordwise distance when the shock is much aft of the leading edge or outboard of the root. In addition to the coarse spacing at the trailing edge, since no transformation was introduced to align the wing trailing edge with a mesh plane, the computational trailing edge is defined by the closest mesh point to the trailing edge. The result is a trailing edge with some discontinuities, referred to as the "zig-zag" trailing edge.

Improvements Incorporated by Douglas. Several improvements to the basic Jameson-Caughey FLO-22 transonic program have been made by Douglas. These improvements include an approximate modeling of finite-fuselage volume effects, introduction of automated input and graphical output procedures, introduction of momentum control volume integrations for separation of the induced drag from the calculated shock drag, and introduction of an extrapolated iteration scheme.

Since the basic FLO-22 program was restricted to wing-alone cases, fuselage flow-field effects were neglected. An approximate modeling of finite-fuselage volume effects has been accomplished by considering the local Mach number change across the wing span due to the isolated fuselage shape. An average local Mach number change is estimated using Hess's higher order axisymmetric potential-flow solution. The wing transonic flow solution is then computed using this higher (or lower) local Mach number as the freestream Mach number. The computed pressure and force coefficients are subsequently re-referenced back to the true freestream Mach number.

For low-wing, transport-type configuration, the side of the fuselage is used as the plane of symmetry to approximate the flow on the upper surface close to the wing root. To account for fuselage lift carry-over, the exposed wing lift coefficient is typically corrected by using a lifting-surface theory calculation.

Input procedures for the J-C FLO-22 program have been automated so that only wing-section geometry and flow conditions are required. The program has also been coupled to graphical output routines. All section pressure distributions and isobars, as well as the three-dimensional geometry, are automatically plotted for each flow solution.

Momentum control-volume integrations were introduced into the FLO-22 program in order to provide a separate evaluation of the calculated induced drag and shock drag. The separate evaluation of these two drag sources provides a check on numerical accuracy and some insight into complicated flows.

The simple extrapolated iteration scheme examined by Jameson and Caughey for axisymmetric flow analysis[15] has been incorporated in the FLO-22 program. This scheme, with adequate protection features, has proven to be quite dependable and provides about a 30-percent reduction in solution computation time for equivalent maximum residual levels.

Computation Time. A typical inviscid-flow computation with the J-C FLO-22 program utilizes 50 iterations on each of three mesh definitions. The final mesh contains 192 x 26 x 32 cells. The solution with the Douglas-incorporated improvements takes approximately 50 CPU minutes on a CYBER 74 or 30 CPU minutes on an IBM 370/165 computer.

3. Calculated and Experimental Results

The two wing configurations selected to use to illustrate the capabilities of the Douglas combined three-dimensional transonic and viscous computational design tool are both high aspect-ratio designs based on the use of airfoils that have a significant amount of aft loading. Some of the geometric characteristics of the two wings are highlighted in the following table:

Wing	$t/c_{\text{Average Exposed}}$	AR	$\Lambda_{c/4}$	Wind Tunnel Test Configuration	
				Fuselage Fineness Ratio	Fuselage Diameter/ Wing Span Ratio
A	∿13.2%	12	30°	7.15	0.131
B	∿12.3%	10.85	30°	∿7.0	0.127

The design goals at high-speed conditions for these wings, in terms of aerodynamic performance characteristics, were a low compressibility drag at cruising conditions, which would be indicative of separation-free flow, and a corresponding buffet boundary high enough to permit cruising at the best lift coefficient consistent with the wing aspect ratio.

The first configuration, Wing A, was designed and a wind-tunnel model of it nearly completed before the FLO-22 version of the Jameson-Caughey (J-C) full-potential program was operational. Just prior to completion of the wind-tunnel model, some initial predictions of the three-dimensional "inviscid" transonic flow-pattern development were obtained using the J-C program. The predicted isobars for the upper surface of the wing, obtained by using a two-dimensional subcritical boundary-layer representation, and accounting for the influence of the fuselage in the manner described in Section 2.2, are shown in Figure 3 for a wing-body

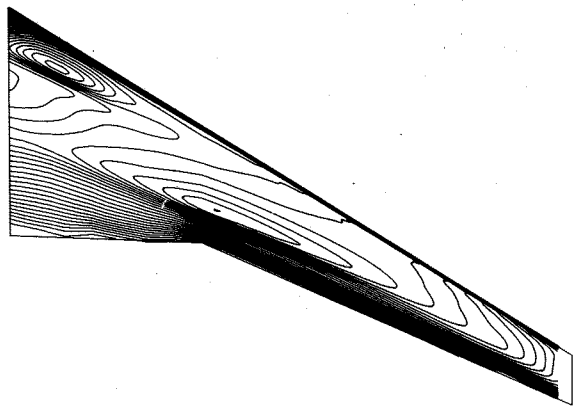

Figure 3. Predicted Upper-Surface Isobars for Wing A at 0.78 Mach Number.

lift coefficient of nearly 0.6 and a freestream Mach number of 0.78. This Mach number was about 0.02 less than the not-too-optimistic target cruise condition. Based on past experience with airfoil separation problems, the predicted pressures gave reason for concern over a likely boundary-layer separation problem in the region of the trailing-edge break station due to the aft location of the shock in this area and the attendant steep adverse pressure gradient from the shock to the trailing edge. This unsweeping and resultant aft location of the shock at the trailing-edge break station was not predicted by the previous design tool which included the Garabedian-Korn two-dimensional transonic program for airfoil development and an incompressible lifting-surface program for finite span effects. Although it appeared from the J-C predictions that this particular wing design was not likely to achieve the target performance, the lack of correlative data between J-C predictions and experimental results for this type of configuration led to the decision to proceed with the test. The test was conducted in early 1977 at a test Reynolds number of 1.9×10^6 based on the mean aerodynamic chord of the wing. Wind-tunnel measured pressures for both the upper and lower surface of the wing are compared in Figure 4 to the J-C predictions for a freestream Mach number of 0.78 at a wing-body lift coefficient of nearly 0.6. At these conditions, the agreement between experimental and predicted pressure distributions, in terms of shock location and strength, as well as the general flow development, is quite good except for some minor discrepancies on the upper surface on the outer part of the wing. These discrepancies may be due to model aeroelastics. This type of good agreement is typical of what we have now become accustomed to for the FLO-22 version of the J-C program. There is, however, one important area in which the agreement between the experimental and J-C predicted pressure distributions is not good. The area of concern is the gradient of the pressure rise through the shock wave. This gradient is smeared out over a much greater chordwise distance in the J-C predictions than it is in reality.

An examination of the trailing-edge pressures at the trailing-edge break station shows that the

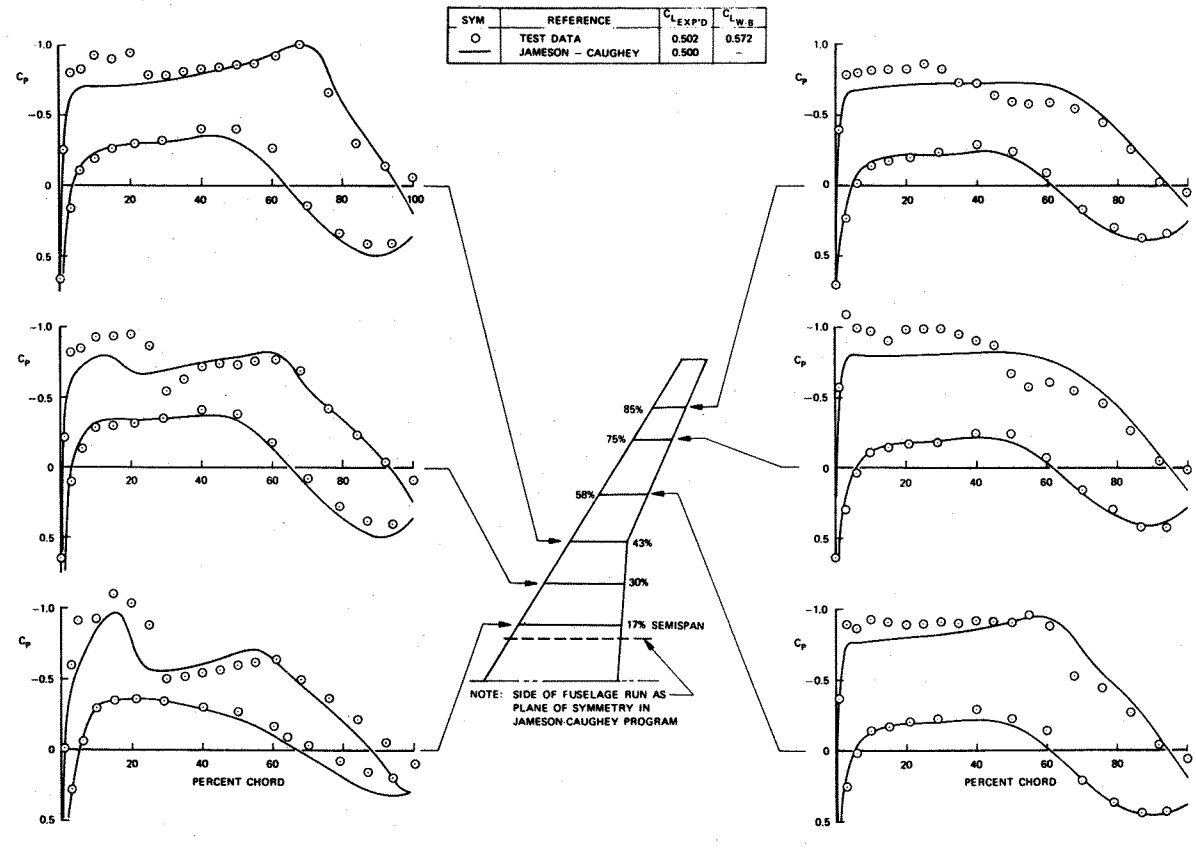

Figure 4. Comparison of Calculated and Experimental Wing Pressure Distributions for Wing A at 0.78 Mach Number.

potential problem indicated by the J-C program did materialize in the form of a local flow separation. The existence of this separation, starting at about 85-percent chord, was apparent from the oil-flow visualization studies conducted at this condition and illustrated in Figure 5. In addition to this separated flow area, a smaller region of separated

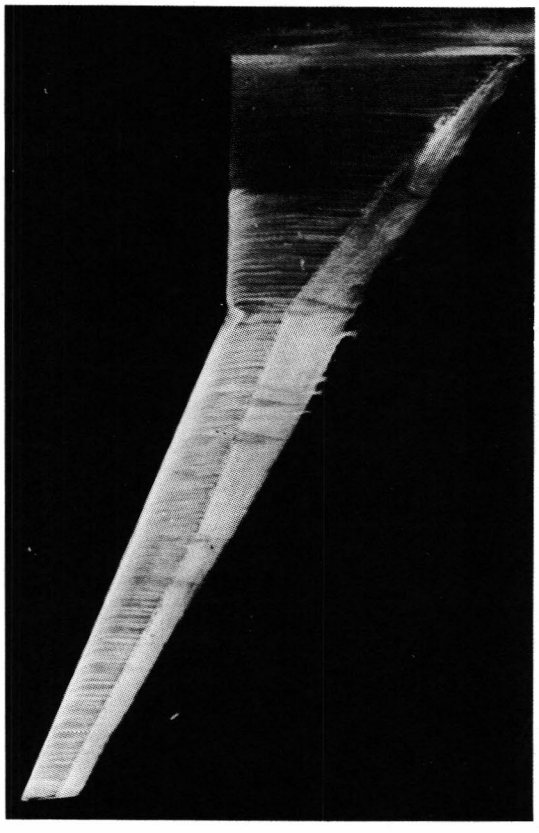

Figure 5. Oil Flow Visualization for Wing A at 0.78 Mach Number.

flow at the trailing edge was observed around the 70-percent semispan location. The effect of these premature separations, particularly the one at the trailing-edge break station, was to reduce the drag rise Mach number for this wing by more than 0.02 below the target performance set for the particular combination of airfoil types, sweep, thickness, and lift coefficient. This degradation is shown in Figure 6.

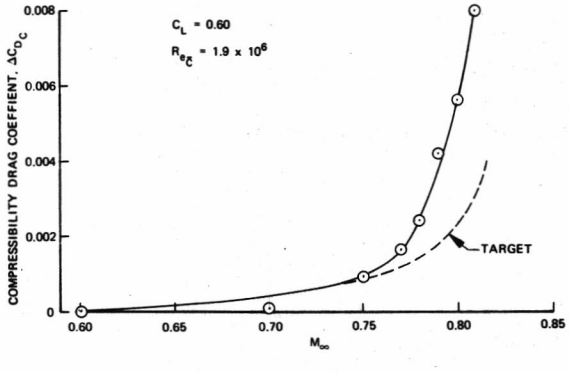

Figure 6. Drag Rise Characteristics of Wing A.

When the new, improved CKR three-dimensional boundary-layer program was coupled with the Jameson-Caughey FLO-22 transonic program, Wing A was one of the first configurations to be analyzed. At the critical 0.78 Mach number condition at the wind-tunnel Reynolds number of 1.9 x 10^6 (based on the mean aerodynamic chord of the wing), boundary-layer separation was predicted right around the 85-percent chord point just outboard of the trailing-edge break station. This compared almost exactly with the experimentally-observed separation point location in this area. An examination of the boundary-layer parameters for this case showed that the CKR program had calculated transition would occur near the 20-percent chord point close to the root, and then automatically used this location, in terms of percent of local wing chord, at all span stations. It can be seen from Figure 5 that this calculated location agrees closely with the observed location near the root, but over most of the rest of the span it is significantly forward of the aft transition location fixed in the wind tunnel to better simulate the flight nondimensional boundary-layer thickness of the shock. The discrepancy between the transition location used in the calculations and that fixed in the wind tunnel is particularly large in the vicinity of the trailing-edge break station where transition in the wind-tunnel was fixed aft of 50-percent chord. Since the capability to set variable-percent-chord transition location across the span was not available at the time, an additional three-dimensional boundary-layer calculation was done, with the transition point fixed right near the leading edge, to determine the effect of moving the transition point on the predicted location of separation. Interestingly enough, there was no change in the predicted separation point. Several two-dimensional boundary-layer calculations with varying-transition location were then made using the J-C predicted pressure distribution at the trailing-edge break station. With transition located near 20-percent chord, as it had been in the three-dimensional boundary-layer calculation, separation was predicted at near 92-percent chord, well aft of the location observed in the wind tunnel and the location predicted with the three-dimensional calculation. As with the three-dimensional calculation, there was almost no change in the predicted separation point when transition was fixed right near the leading edge. However, when the transition point was moved further aft to near the wind-tunnel test location, the separation point predicted two-dimensionally moved aft to essentially the trailing edge, clearly indicating that the two-dimensional strip-theory approximation is not adequate for this application. Presuming that the separation point predicted by the three-dimensional CKR method would also move aft a similar distance (but not to the trailing edge) as the transition point is moved aft to the wind-tunnel location, it is estimated that the three-dimensional predicted separation point with the correct transition location would be somewhat aft of the observed separation point, but well forward of the wing trailing edge. A predicted separation point somewhat aft of the observed separation point is not unexpected due to the too-gradual adverse pressure gradients predicted for shocks by the J-C method.

The three-dimensional boundary-layer skin-friction characteristics predicted for Wing A at 0.78 Mach number and at the wind-tunnel-test

Reynolds number are compared in Figure 7 at several semispan locations to the comparable predictions obtained using the two-dimensional strip-theory approximation. Transition is set at about 20-percent chord for both calculations. The two-dimensional predictions with this transition location indicate separation would occur all across the span, being most critical at the trailing-edge break station. However, the predicted separation is eliminated all across the span when the further-aft wind-tunnel-test transition location is used in the calculations. With the three-dimensional boundary-layer calculations, the separation at the trailing-edge break station is predicted to occur further forward, and hence is not likely to be eliminated with the further-aft transition location. When the three-dimensional calculations predicted separation at about the 85-percent-chord point at the trailing-edge break station, the calculations did not continue outboard. Therefore, there is no prediction of any outboard separation. However, it can be seen that the tendency to predict separation is significantly greater with the three-dimensional calculations, and consequently the three-dimensional prediction with the appropriate transition location is much more likely to predict the separation that occurred at 70-percent semispan in the wind tunnel.

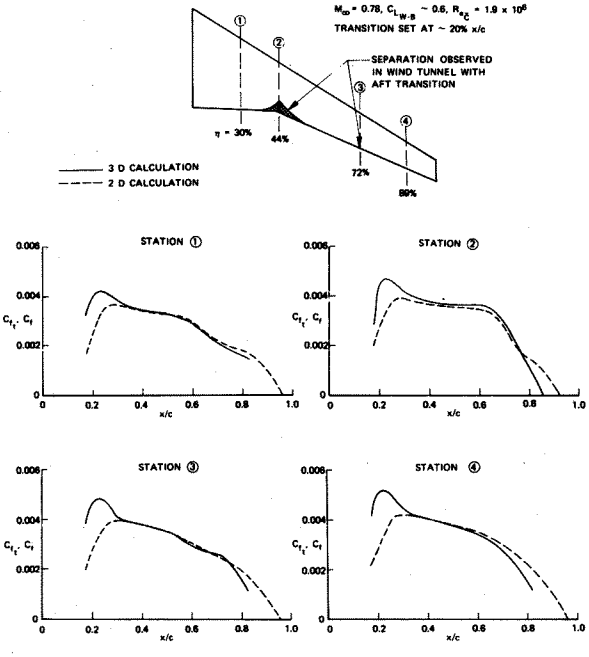

Figure 7. Comparison of Two- and Three-Dimensional Predicted Skin-Friction Characteristics for Wing A at Wind-Tunnel Reynolds Number.

Both the two- and three-dimensional boundary-layer calculations for Wing A at this Mach number were repeated using a much higher typical flight Reynolds number. Transition for these calculations was set right near the leading edge. The predicted boundary-layer skin-friction and displacement thickness (and surface) characteristics are shown in Figure 8. The two-dimensional-strip calculations predict separation only at the trailing-edge break station. In contrast, the three-dimensional

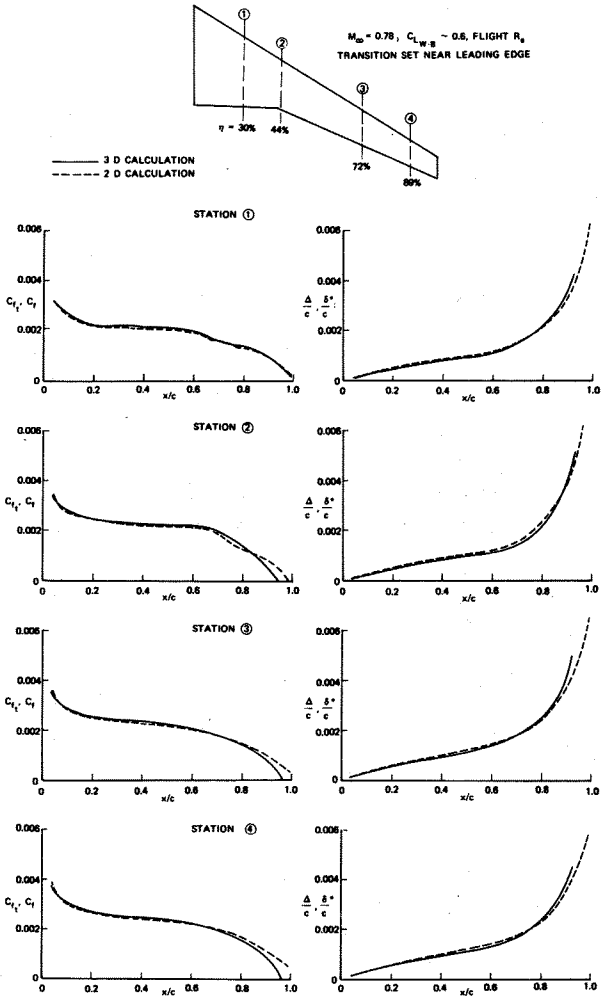

Figure 8. Comparison for Two- and Three-Dimensional Predicted Boundary-Layer Characteristics for Wing A at Flight Reynolds Number.

calculations indicate separation would occur near the trailing edge over most of the span from the trailing-edge break station outboard. One interesting aspect of the predicted three-dimensional displacement surface characteristics compared to the predicted two-dimensional displacement thickness is the more rapid rate of growth of the surface height over the aft portion of the airfoil. This greater rate of increase would result in more viscous decambering of the aft-loaded airfoil.

At the conclusion of the wind-tunnel test of Wing A, an intense systematic study using the J-C FLO-22 program was undertaken to determine what geometric changes were required to suppress the development of the strong aft shock over the inboard portion of the wing as seen on Wing A. Over a period of approximately 20 weeks, 40 different wing configurations were investigated. This involved nearly 100 flow solutions with the J-C program. The effects of planform, airfoil type,

thickness, and twist variations were systematically determined. It was found that in order to suppress the development of the strong aft shock over the inboard part of the wing, careful tailoring of thickness, planform trailing edge sweep and airfoils was required. For example, an increase in chord at the trailing-edge break station of Wing A was fundamental to effecting an improvement in the three-dimensional flow characteristics over the inboard panel. A somewhat lower thickness ratio in the inboard region was also determined to be essential. The use of an inboard leading-edge extension gave a significant improvement through elimination of the inboard shock by a reduction in section lift coefficient and an increase in isobar sweep. Other effects investigated included variations in airfoil leading-edge and aft-camber geometries to determine the effects on drag "creep" prior to cruise Mach number, drag-divergence Mach number, and buffet-onset lift capability. One of the configurations selected from this study to be wind-tunnel tested is referred to as Wing B in this paper. Wing B is quite different than Wing A. The most obvious changes include a significantly different planform and a slightly reduced overall thickness ratio. The reduction in thickness ratio by itself should theoretically result in a 0.01 increase in the drag-rise Mach number.

The J-C predicted isobars for the upper surface of Wing B at a freestream Mach number of 0.80 and a wing-body lift coefficient of 0.55, are shown in Figure 9. It can be seen that there is no aft shock predicted as occurred with Wing A, but only a relatively weak shock forward on the wing. The unsweeping of the isobars over the inner part

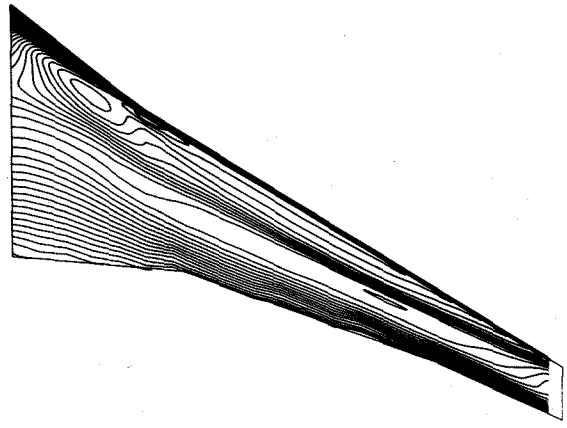

Figure 9. Predicted Upper-Surface Isobars for Wing B at 0.8 Mach Number.

of the wing that occurred with Wing A has also been corrected. To verify the predicted improvement, this configuration was tested earlier this year at a test Reynolds number of 5.4×10^6 based on the mean aerodynamic chord of the wing. A comparison of the predicted and experimental pressure distributions at 0.80 Mach number is presented in Figure 10. For this condition, the agreement is not quite as good as it was with Wing A in that the actual forward shock is somewhat stronger than the predicted shock. However, other than that

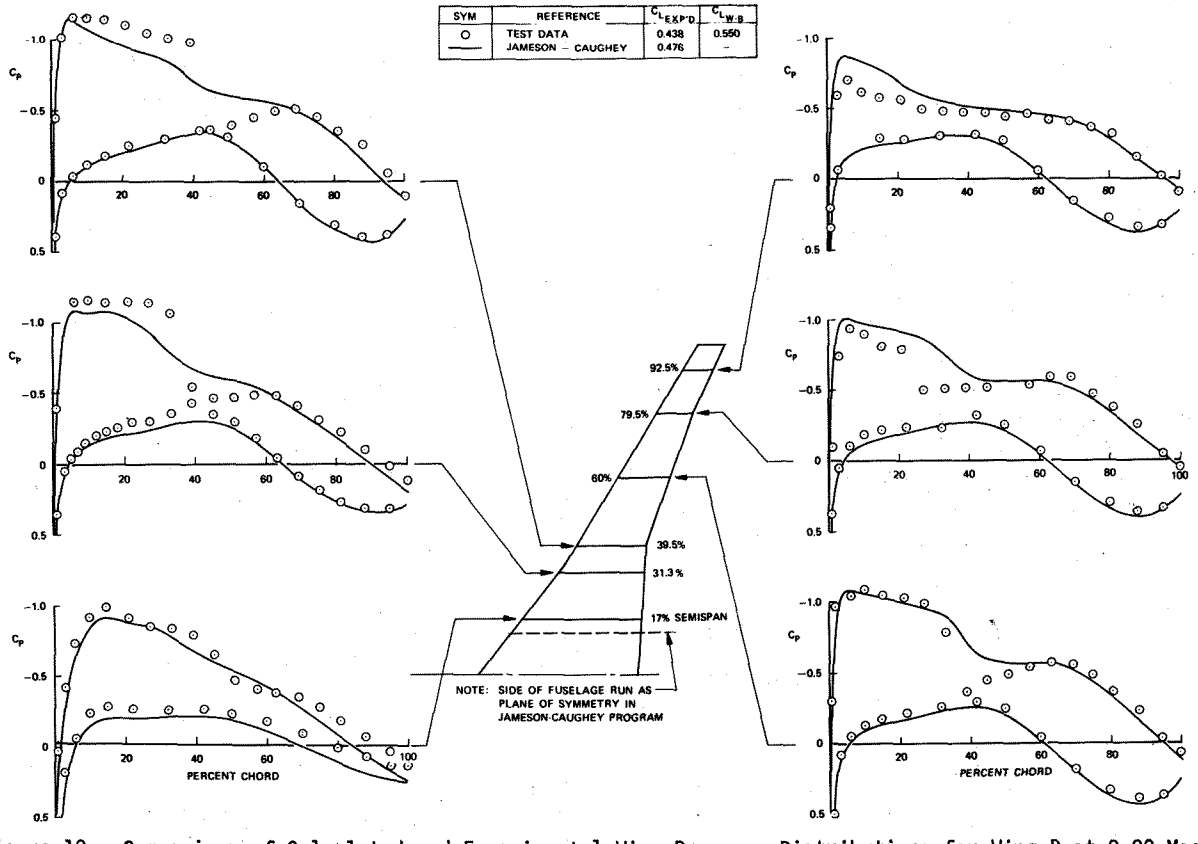

Figure 10. Comparison of Calculated and Experimental Wing Pressure Distributions for Wing B at 0.80 Mach Number.

discrepancy, and the problem near the tip, the general character of the flow development is predicted quite well. The improvement in the wing flow pattern for Wing B relative to that of Wing A resulted in the marked improvement in the drag rise characteristics illustrated in Figure 11.

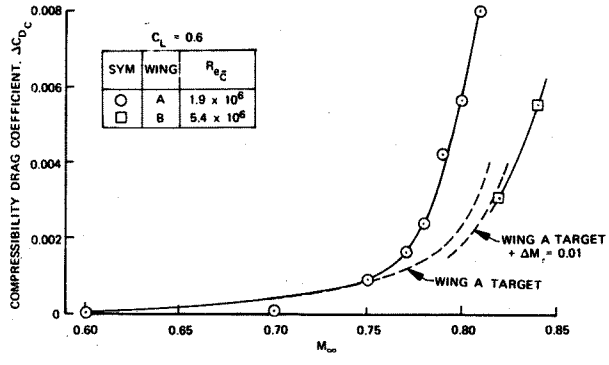

Figure 11. Drag Rise Characteristics of Wing B Relative to Wing A.

The two- and three-dimensional boundary-layer skin-friction characteristics predicted for Wing B at 0.8 Mach number and at a typical flight Reynolds number are shown in Figure 12. It can be seen that neither the two- or three-dimensional calculations predict any separation near the trailing edge. There is little difference between the two calculation methods for this configuration with its relatively mild pressure gradients. The only noticeable difference is the slightly-more-rapid decrease

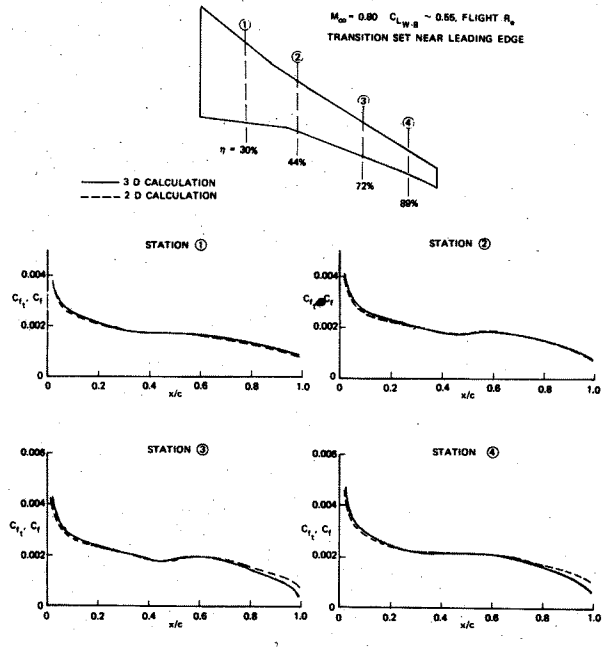

Figure 12. Comparison of Two- and Three-Dimensional Predicted Skin-Friction Characteristics for Wing B at Flight Reynolds Number.

in the three-dimensional skin-friction coefficient near the trailing edge due to the spanwise flow component in this region.

4. Areas Requiring Further Study

The capability demonstrated by the calculated results obtained with the current version of the coupled CKR and J-C programs provides a very powerful and useful aerodynamic design tool. This current capability represents a very significant step toward the goal of being able to accurately predict the total drag (viscous and invsicid) at cruising conditions, and the onset of trailing-edge separation (buffet onset), for three-dimensional wing-body combinations at transonic conditions. However, there are several areas where additional studies need to be done before the desired capabilities can be fully achieved. Included among the areas for additional study are the following:

● Finite Fuselage Representation. The current accountability for the effect of a finite length fuselage on the wing flow field in the Douglas version of the J-C program is based on using the average Mach number increase across the wing span predicted by considering the isolated fuselage shape. While this correction is probably a reasonable first-order approximation, it is very likely that, in reality, the propagation of the fuselage effect along the wing span may be magnified by the presence of supercritical flow on the wing. Development of the capability to specifically handle the interaction between a wing and a finite-length fuselage is being pursued by Jameson and Caughey who are adding this capability to the conservative, finite-volume version of their transonic-flow program.

● Shock-Wave-Boundary-Layer Interaction. It is necessary to appropriately model the shock-wave-boundary-layer interaction region in the computational methods in order to account for both the effect that the local boundary-layer behavior has on the shock strength and location, and to be able to define the boundary-layer state at the exit from the interaction region. The latter is necessary so that the boundary-layer calculations can be correctly continued downstream to the trailing edge of the wing for the desired prediction of displacement, drag, and separation characteristics. With regard to the effect of the local boundary-layer behavior on the shock strength and location, recent experience has shown that the shock strengths and positions predicted by the conservative, finite-volume version of the J-C program, without any accounting for this interaction effect, do not match experimental results nearly as well as with the nonconservative FLO-22 version. Some preliminary studies indicate that simulating this interaction in the fully conservative programs will overcome this problem. Since the conservative, finite-volume version of the J-C program is felt to be more correct than the nonconservative version, and is the version that will have the capability to account for a finite-length fuselage, an appropriate interaction model will have to be developed.

One problem that stands in the way of being able to correctly calculate the boundary-layer state at the exit from the interaction is that the J-C inviscid representation of the shock-wave pressure gradient is smeared over a much greater chordwise distance than actually occurs. The shock jump, from the point of maximum Mach number to a point

where the flow is slightly subcritical, is spread over a distance (several computational mesh widths) that is well in excess of 10 percent of the local wing chord in many cases. Depending on the spanwise location, Reynolds number, and shock location, this distance over which the shock jump is spread can easily be 20 or more local boundary-layer thicknesses. This is in contrast to a distance of the order of 5 or 6 boundary-layer thicknesses that has been previously shown as being required to match experimental results at moderate shock strengths. To illustrate the effect that this nonrepresentative smearing has on the calculated boundary-layer characteristics, the skin friction and displacement thickness characteristics predicted with the two-dimensional version of the CKR method are shown in Figure 13 for the upper surface of an aft loaded airfoil configuration at a condition that was approaching trailing-edge separation experimentally. The shock Mach number of 1.27 is close to that for which a separation bubble should occur at the foot of the shock. The pressure distributions used are experimental measurements except right in the region of the shock where they are modified to permit a variation in the smearing effect. With the shock smeared over 20 boundary-layer thicknesses, the predicted skin-friction characteristics at the end of the shock pressure gradient show no tendency toward separation. At 6 boundary-layer thicknesses, the predicted boundary layer is just about separated as it should be. The calculated boundary-layer displacement thickness at the airfoil trailing edge when the shock pressure gradient is spread over 6 boundary thicknesses is nearly 50 percent greater than it is when the pressure gradient is spread over 20 boundary-layer thicknesses. This difference in the calculated displacement thickness would be magnified even more if the trailing-edge calculation were handled correctly.

The impact of the shock pressure-gradient smearing on the calculated boundary-layer characteristics for the same airfoil at conditions closer to typical cruise operation are illustrated in Figure 14. Here, where the shock is further forward, and there is more distance for the boundary layer to recover from the effect of the shock prior to encountering the adverse pressure gradient over the aft part of the airfoil, there is less effect on the boundary-layer condition approaching the trailing edge. However, the effect is still not trivial. The impact of the shock smearing on the calculated profile (viscous) drag for this condition is shown in Figure 15. There is more than a 15-percent difference in the calculated drag for the airfoil upper surface due to the smearing of the shock pressure gradient.

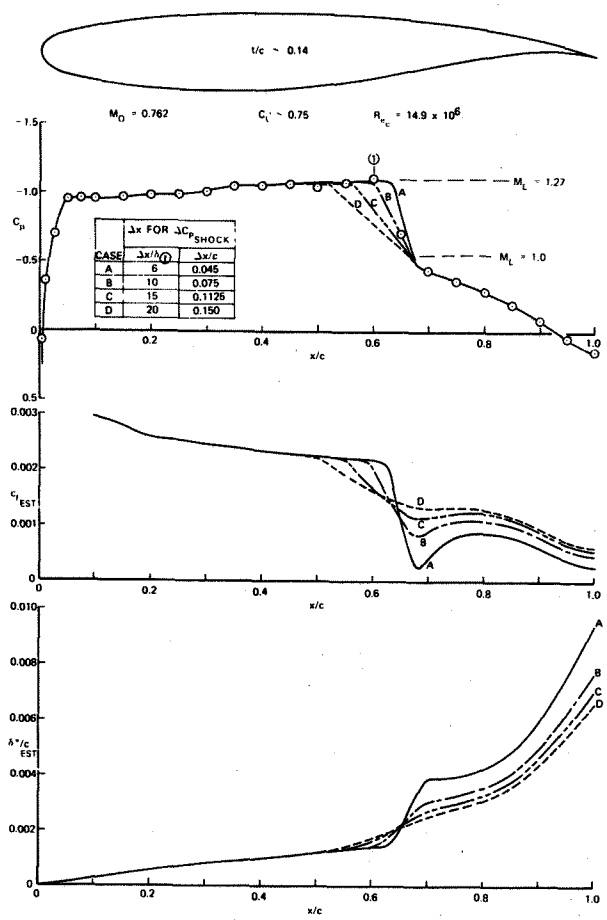

Figure 13. Effect of Shock Pressure-Gradient Smearing on Calculated Boundary-Layer Characteristics for an Airfoil at Conditions Close to Trailing-Edge Separation.

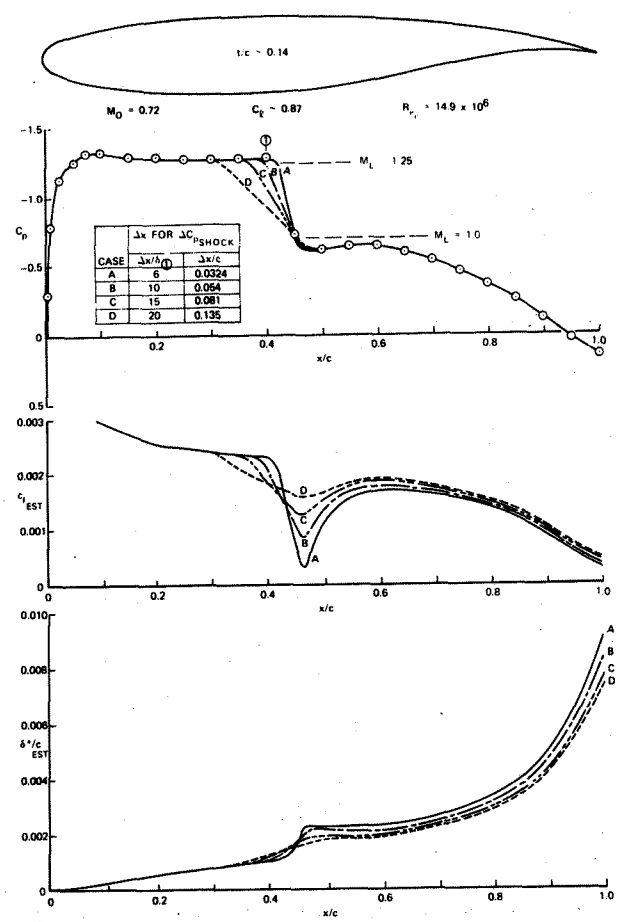

Figure 14. Effect of Shock Pressure-Gradient Smearing on Calculated Boundary-Layer Characteristics for an Airfoil at Condition Close to Cruise.

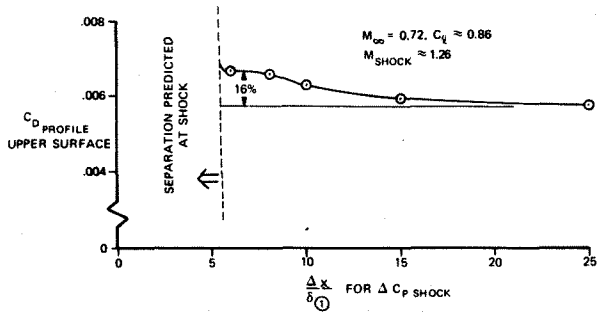

Figure 15. Effect of Shock Pressure Gradient Smearing on Calculated Profile Drag.

In order to overcome the difficulty with the smeared shock pressure gradient in the development of an appropriate interaction model, it will be necessary to investigate means to sharpen up the inviscid pressure gradient so that the true smearing produced by the boundary layer can be calculated. Many more LDA measurements of the inviscid and boundary-layer characteristics in the interaction region will also be required to help guide the development of the interaction model, particularly for weak or moderate shock strengths ($M_L \leq 1.3$), for which there is essentially no data available. The development of an interaction model and the related experimental investigations will initially be confined to two-dimensional flows, but will eventually have to be extended to three-dimensional swept environments.

● Trailing-Edge-Wake Interaction. It has been shown[16] that wake curvature and static-pressure variations across the boundary layer in the trailing-edge region of an airfoil have a large effect on the viscous contribution to lift. However, it is probably at least as important that the trailing edge-wake interaction be correctly accounted for in the prediction of airfoil (and wing) drag and trailing-edge boundary-layer separation. To illustrate how sensitive the boundary-layer calculations near the trailing edge are to details, calculations were made at the same conditions as those shown in Figure 13, but this time with the trailing-edge pressure coefficient increased by 0.05. The results, portrayed in Figure 16, show how this small change modified the calculated boundary-layer characteristics near the trailing-edge from indicating no separation to now predicting separation, and resulted in large increases in the calculated boundary-layer displacement thickness. This illustration also shows the difficulty of trying to match measured boundary-layer characteristics with calculations based on experimental pressure distributions, particularly when the flow at the trailing edge is separated or even near separation. The reduction in the rate of decrease of the calculated local skin friction near the trailing edge, based on the experimental pressure distribution, is closely related to the classic textbook example when a separation exists. In that case, boundary-layer calculations made using the experimental pressure distributions show a decrease in skin-friction coefficient as the separation point is approached, but then start to increase.

The development of a method for calculating the trailing edge-wake interaction region is far from being straightforward. Several problems need to be addressed. They include:

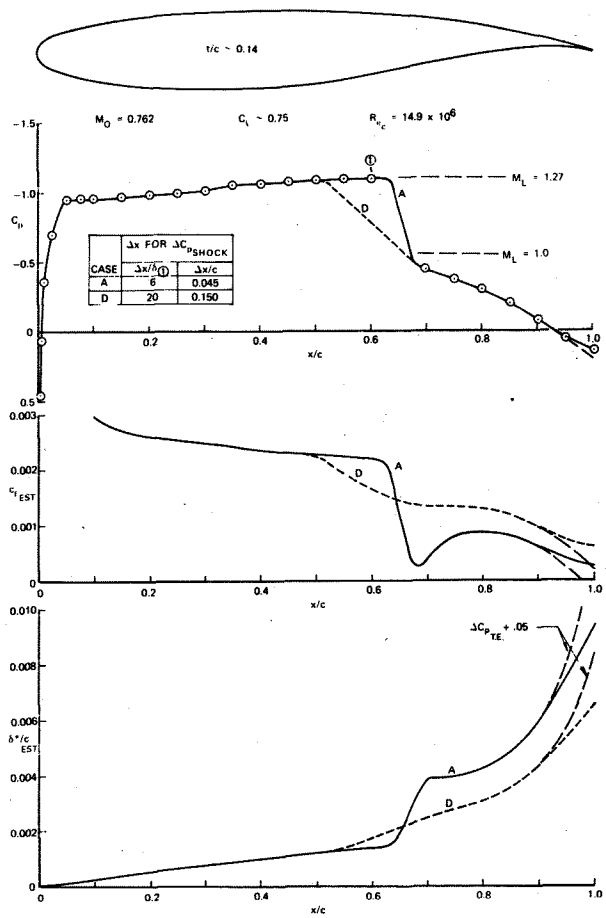

Figure 16. Effect of Change in Trailing-Edge Pressure on Calculated Boundary-Layer Characteristics for an Airfoil at Conditions Close to Trailing-Edge Separation.

(1) The interaction between the viscous and potential flow requires careful consideration and may prove to be the most important aspect of this development.

(2) The degree to which boundary-layer equations can be used to represent this problem must be determined.

(3) The need to account for turbulence details, and the manner in which this is done, requires further investigation.

(4) The Jameson-Caughey method will have to be modified to better represent conditions at the trailing edge.

(5) LDA experimental measurements are needed for different airfoil types in order to define the flow characteristics, including turbulence quantities, near the trailing edge, and in the wake, to help guide the development of the interaction model.

(6) When the problem is in hand for two-dimensional flows, it will have to be extended to three-dimensional flows accounting for such effects as the spanwise flow in the wake measured by Michel et al[17].

● Turbulence Models. In addition to the probable need to develop higher turbulence models involving the transport of turbulence energy to represent flows far from equilibrium such as shock-wave-

boundary-layer interactions and the trailing-edge-near-wake region, it may be necessary to use a higher turbulence model to more accurately represent the flow in the strong adverse pressure gradient found on the upper aft part of airfoils, particularly aft-loaded airfoils. The question to be answered is- which higher-order model is most appropriate to which flow? Much experimental work will be needed to answer this question. Initial testing will be for two-dimensional flows. Eventually the spanwise flow influence for three-dimensional flows will have to be defined.

• Calculation of Boundary-Layer Flow Characteristics through Small Regions of Separated Flow. Although the current goal for the coupled CKR and J-C programs does not include calculation through significant regions of separation, it will be necessary to incorporate in the three-dimensional CKR boundary-layer method the capability to handle flows with separation bubbles that reattach, and small regions of separation. A typical case where the boundary-layer flow can have a separation bubble and then reattach occurs at the shock wave-boundary-layer interaction on the upper surface of an aft-loaded airfoil when it is operating beyond the cruise point but prior to trailing-edge separation (buffet). An example of a case where it would be necessary to continue the boundary-layer calculations through small regions of separated flow occurs when a wing configuration being analyzed has more than one critical area for separation across the wing span. The spanwise marching will only permit identification of the most inboard one.

• Calculation of Corner Flows. Flight and wind tunnel flow visualization studies on representative transport aircraft have clearly shown that separation due to the viscous effect in flows along axial corners represent the largest single source of excess drag at cruise conditions on current configurations. Flow separation problems have been encountered on several aircraft at the wing-fuselage juncture, as well as in other areas. In order to avoid these sources of excess drag on future designs, it is necessary to formulate and develop a method to accurately calculate the boundary-layer flow in these regions. This will also provide a more reliable prediction of initial boundary-layer profiles along the root chord than those currently obtained by using tapered-wing equations.

5. Conclusions

A new, improved version of the Cebeci-Kaups-Ramsey (CKR) three-dimensional finite-difference boundary-layer program for arbitrary wings has been coupled with the Jameson-Caughey FLO-22 full potential transonic flow method to predict the combined viscous/inviscid flow characteristics of three-dimensional swept wings of transonic conditions. The resulting coupled program provides a very powerful and useful aerodynamic design tool. Results of some preliminary calculations are presented for two advanced transport wing configurations. One of the configureations had a separation problem at cruising conditions, while the second, developed using the J-C transonic method, avoided any separation problems at cruising conditions. The main conclusions to be drawn from the calculations performed to date include the following:

• The Jameson-Caughey FLO-22 transonic full potential method correctly calculates the general flow development and overall three-dimensional pressure distributions for relatively thick advanced-transport-type wing configurations at transonic conditions. The capability afforded by the J-C method has been used to identify the effects of geometry changes in the design of a three-dimensional high-aspect-ratio wing that achieved the target drag rise Mach number.

• The new, improved CKR three-dimensional boundary-layer method provides a much more realistic estimate of the boundary-layer characteristics which exist on three-dimensional swept wing configurations that have strong adverse pressure gradients and/or are near separation than is obtained with the two-dimensional strip-theory approximation. The occurrence of separation on a wind-tunnel model of a high-aspect ratio wing has been predicted by the three-dimensional method, whereas the strip-theory approximation is shown to be overly optimistic for both the prediction of boundary-layer separation and the viscous decambering effect of the boundary-layer displacement surface on aft-loaded airfoils.

• Several areas have been identified where additional studies need to be conducted in order to develop this design tool into an even more useful design tool. These include the need to account for a finite-fuselage configuration, the need to better model the shock-wave-boundary-layer interaction, the need to better model the trailing-edge-wake interaction, the need to develop higher turbulence models, the need to calculate boundary-layer flow characteristics through small regions of separated flow, and the need to calculate flows along axial corners.

Acknowledgment

The author wishes to express his appreciation to T. Cebeci, K. Kaups and the other members of the Douglas Aerodynamics Research Group, and to P. A. Henne of the Douglas Aerodynamics Technology Programs Group, for their helpful discussions and assistance in providing the calculations used in this paper.

References

1. Henne, P.A. and Hicks, R.M.: Transonic Wing Analysis Using Advanced Computational Methods, AIAA Paper 78-105, 1978.

2. Chen, A., Tinoco, E., and Yoshihara, H.: Transonic Computational Design Modifications of the F-111 TACT, AIAA Paper 78-106, 1978.

3. Mason, W., MacKenzie, D.A., Stern, M.A. and Johnson, J.K.: A Numerical Three-Dimensional Viscous Transonic Wing-Body Analysis and Design Tool, AIAA Paper 78-101, 1978.

4. Jameson, A. and Caughey, D.A.: Numerical Calculation of the Transonic Flow Past a Swept Wing, New York University ERDA Report COO-3017-140, 1977.

5. Cebeci, T., Kaups, K., and Ramsey, J.A.: A General Method for Calculating Three-Dimensional Compressible Laminar and Turbulent Boundary Layers on Arbitrary Wings, NASA CR-2777, 1977.

6. McLean, J.D.: Three-Dimensional Turbulent Boundary-Layer Calculations for Swept Wings, AIAA Paper 77-3, 1977.

7. Kordulla, W.: Inviscid-Viscous Interaction in Transonic Flows about Finite Three-Dimensional Wings, AIAA Paper 77-209, 1977.

8. Nash, J.F. and Scruggs, R.M.: An Implicit Method for the Calculation of Three-Dimensional Boundary Layers on Finite Thick Wings, AFFDL TR-77-122, Vol. III, 1977.

9. Cebeci, T.: Calculation of Three-Dimensional Boundary Layers, I. Swept Infinite Cylinders and Small Cross Flow, AIAA J., Vol. 12, June 1974, pp. 779-786.

10. Keller, H.B. and Cebeci, T.: Accurate Numerical Methods for Boundary Layers, II. Two-Dimensional Turbulent Flows, AIAA J., Vol. 10, Sept. 1972, pp. 1197-1200.

11. Cebeci, T. and Bradshaw, P.: Momentum Transfer in Boundary Layers, McGraw-Hill/Hemisphere Book Co., 1977.

12. Moore, F.K.: Displacement Effect of a Three-Dimensional Boundary Layer, NACA Report 1124, 1953.

13. Ballhaus, W.F., Bailey, F.R., and Frick, J.: Improved Computational Treatment of Transonic Flow About Swept Wings, Advanced in Engineering Sciences, Vol. 4, 1976, pp. 1311-1320.

14. Boppe, C.W.: Calculation of Transonic Wing Flows by Grid Embedding, AIAA Paper 77-207, 1977.

15. Caughey, D.A. and Jameson, A.: Accelerated Iterative Calculation of Transonic Nacelle Flow Fields, AIAA Paper 76-100, 1976.

16. Melnick, R.E., Chow, R., and Mead, H.R.: Theory of Viscous Transonic Flow Over Airfoils at High Reynolds Numbers, AIAA Paper 77-680, 1977.

17. Michel, R., Mignosi, A., and Quemard, C.: The Induction Driven Tunnel T2 at ONERA-CERT: Flow Qualities, Testing Techniques and Examples of Results, AIAA Paper 78-767, 1978.